YIPF6 controls sorting of FGF21 into COPII vesicles and promotes obesity

Lirui Wang[a,b,c,1,2], Magdalena Mazagova[b,1], Chuyue Pan[a,1], Song Yang[d,1], Katharina Brandl[e], Jun Liu[a], Shannon M. Reilly[b], Yanhan Wang[b], Zhaorui Miao[a], Rohit Loomba[b], Na Lu[a], Qinglong Guo[a], Jihua Liu[f], Ruth T. Yu[g], Michael Downes[g], Ronald M. Evans[g,h], David A. Brenner[b], Alan R. Saltiel[b], Bruce Beutler[i,2], and Bernd Schnabl[b,c,2]

[a]School of Basic Medicine and Clinical Pharmacy, China Pharmaceutical University, 211198 Nanjing, Jiang Su, China; [b]Department of Medicine, University of California San Diego, La Jolla, CA 92093; [c]Department of Medicine, VA San Diego Healthcare System, San Diego, CA 92161; [d]Department of Hepatology, Beijing Ditan Hospital, Capital Medical University, Chaoyang District, 100015 Beijing, China; [e]Skaggs School of Pharmacy and Pharmaceutical Sciences, University of California San Diego, La Jolla, CA 92093; [f]School of Traditional Chinese Pharmacy, China Pharmaceutical University, 211198 Nanjing, Jiang Su, China; [g]Gene Expression Laboratory, Salk Institute for Biological Studies, La Jolla, CA 92037; [h]Howard Hughes Medical Institute, Salk Institute for Biological Studies, La Jolla, CA 92037; and [i]Center for the Genetics of Host Defense, University of Texas Southwestern Medical Center, Dallas, TX 75390

Contributed by Bruce Beutler, June 4, 2019 (sent for review March 18, 2019; reviewed by Ali Canbay and Wen-Xing Ding)

Fibroblast growth factor 21 (FGF21) is an endocrine hormone that regulates glucose, lipid, and energy homeostasis. While gene expression of FGF21 is regulated by the nuclear hormone receptor peroxisome proliferator-activated receptor alpha in the fasted state, little is known about the regulation of trafficking and secretion of FGF21. We show that mice with a mutation in the Yip1 domain family, member 6 gene (*Klein–Zschocher* [*KLZ*]; *Yipf6*$^{KLZ/Y}$) on a high-fat diet (HFD) have higher plasma levels of FGF21 than mice that do not carry this mutation (controls) and hepatocytes from *Yipf6*$^{KLZ/Y}$ mice secrete more FGF21 than hepatocytes from wild-type mice. Consequently, *Yipf6*$^{KLZ/Y}$ mice are resistant to HFD-induced features of the metabolic syndrome and have increased lipolysis, energy expenditure, and thermogenesis, with an increase in core body temperature. *Yipf6*$^{KLZ/Y}$ mice with hepatocyte-specific deletion of FGF21 were no longer protected from diet-induced obesity. We show that YIPF6 binds FGF21 in the endoplasmic reticulum to limit its secretion and specifies packaging of FGF21 into coat protein complex II (COPII) vesicles during development of obesity in mice. Levels of YIPF6 protein in human liver correlate with hepatic steatosis and correlate inversely with levels of FGF21 in serum from patients with nonalcoholic fatty liver disease (NAFLD). YIPF6 is therefore a newly identified regulator of FGF21 secretion during development of obesity and could be a target for treatment of obesity and NAFLD.

obesity | YIPF6 | FGF21 | COPII vesicles | sorting receptor

According to the World Health Organization, ∼39% of adults were overweight worldwide in 2016; among these, 13% were obese (1). Obesity-related deaths are predominantly due to the development of cardiovascular disease and nonalcoholic fatty liver disease (NAFLD) (1–3). NAFLD has become a leading cause of chronic liver disease with the growing obesity pandemic (3), and liver cells contribute to the progression of obesity. The hepatocyte secretome changes during obesity. Steatotic hepatocytes produce factors that promote or protect against inflammation and insulin resistance (4).

Fibroblast growth factor 21 (FGF21) belongs to the endocrine subfamily of FGFs. Unlike the majority of FGFs, which bind heparan sulfate and become predominantly entrapped within the extracellular matrix of their site of synthesis, FGF21 enters circulation upon secretion due to its diminished heparan sulfate binding, and instead relies on a tertiary receptor complex composed of beta-klotho and FGF receptor 1 (FGFR1) for tissue targeting and signal transduction (5–7). Circulating FGF21 is a primarily hepatocyte-derived hormone in response to fasting or starvation, which exerts its function in a variety of tissues, including white and brown adipose tissue, liver, pancreas, and brain (8–10).

Administration of recombinant FGF21 improves metabolic homeostasis in obese and diabetic mouse models, decreasing plasma glucose and triglycerides (11), increasing insulin sensitivity (12), reducing hepatic steatosis (13), increasing energy expenditure, and decreasing body weight (14, 15). These results suggest that FGF21 might be a promising antidiabetic therapy in humans. Indeed, LY2405319, an engineered variant of FGF21, reduces body weight and dyslipidemia and alters atherogenic apolipoprotein profiles of patients with obesity and type 2 diabetes (16). While delivering engineered recombinant FGF21 variants is a dominant strategy to exploit the therapeutic potential of FGF21, efforts are also underway to boost endogenous FGF21 level or efficacy as an alternative therapeutic strategy, such as using fibroblast-activating protein inhibitors (17) and gene therapy-mediated FGF21 overexpression in liver via adeno-associated virus serotype 8 (AAV8) (18). FGF21 has an amino-terminal signal peptide (leader sequence) and is delivered to the cell surface through the endoplasmic reticulum (ER) to the Golgi (19). However, the mechanisms of FGF21 secretion remain elusive.

Yip1 domain family, member 6 (YIPF6) belongs to a family of proteins comprising YIPF1 through YIPF7. Little is known about the functions of these proteins in mammalian cells (20). The yeast homologs of mammalian YIPFs, named Yips, are membrane receptors for YPT and RAB guanosine triphosphatases (GTPases) and associate with secretory vesicles between the ER and Golgi

Significance

Fibroblast growth factor 21 (FGF21) is an endocrine hormone that regulates glucose, lipid, and energy homeostasis. To date, little is known about the regulation of trafficking and secretion of FGF21. Here, we show that mice with a mutation in the *Yipf6* gene (*Klein–Zschocher* [*KLZ*]; *Yipf6*$^{KLZ/Y}$) on a high-fat diet (HFD) have higher plasma levels of FGF21 than control mice due to the increased FGF21 secretion from their hepatocytes. *Yipf6*$^{KLZ/Y}$ mice are thus resistant to HFD-induced features of the metabolic syndrome. The regulation of YIPF6 on FGF21 secretion was also conserved in nonalcoholic fatty liver disease (NAFLD) patients. YIPF6 is therefore a newly identified regulator of FGF21 secretion during development of obesity and could be a target for treatment of obesity and NAFLD.

Author contributions: L.W., B.B., and B.S. designed research; M.M., C.P., Jun Liu, S.M.R., Y.W., and Z.M. performed research; S.Y., K.B., R.L., N.L., Q.G., and Jihua Liu contributed new reagents/analytic tools; R.T.Y., M.D., R.M.E., D.A.B., and A.R.S. analyzed data; and L.W., B.B., and B.S. wrote the paper.

Reviewers: A.C., University of Magdeburg; and W.-X.D., The University of Kansas Medical Center.

Conflict of interest statement: B.B. received salary support from Pfizer, Inc. B.S. is consulting for Ferring Research Institute.

[1]L.W., M.M., C.P., and S.Y. contributed equally to this work.

[2]To whom correspondence may be addressed. Email: wanglirui@cpu.edu.cn, bruce.beutler@UTSouthwestern.edu or beschnabl@ucsd.edu.

This article contains supporting information online at www.pnas.org/lookup/suppl/doi:10.1073/pnas.1904360116/-/DCSupplemental.

Published online July 9, 2019.

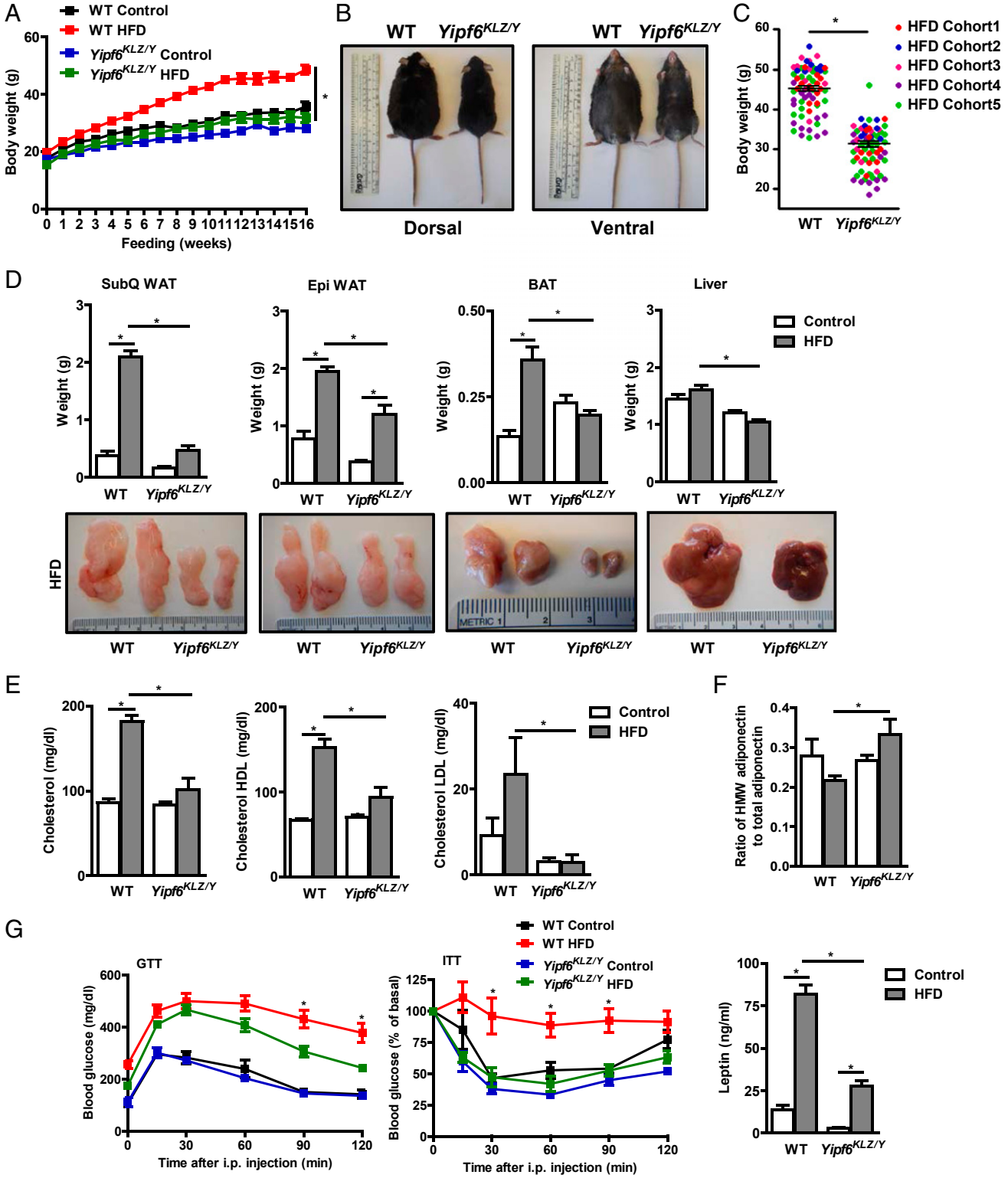

Fig. 1. *Yipf6* mutation protects mice from diet-induced obesity. (*A*) Body weight ($n = 4$ to 5 for control diet and $n = 8$ to 10 for HFD). (*B*) Representative images of WT and *Yipf6*$^{KLZ/Y}$ mice placed on the HFD for 16 wk. (*C*) Body weights of groups ($n = 70$ WT mice fed the HFD and $n = 69$ *Yipf6*$^{KLZ/Y}$ mice fed the HFD). (*D*, *Top*) Weight of s.c. white adipose tissue (SubQ WAT; $n = 8$ to 11 for control diet and $n = 18$ to 22 for HFD), epididymal white adipose tissue (Epi WAT; $n = 8$ to 11 for control diet and $n = 18$ to 23 for HFD), brown adipose tissue (BAT; $n = 5$ for control diet and $n = 5$ to 7 for HFD), and liver ($n = 8$ to 11 for control diet and $n = 18$ to 23 for HFD). (*D*, *Bottom*) Representative images of SubQ WAT, Epi WAT, BAT, and liver from WT and *Yipf6*$^{KLZ/Y}$ mice following the HFD. (*E*) Total, HDL, and LDL cholesterol in plasma ($n = 4$ to 6 for control diet and $n = 5$ for HFD). (*F*) Ratio of high-molecular-weight (HMW) adiponectin to total adiponectin (*Top*) and leptin (*Bottom*) in plasma from WT and *Yipf6*$^{KLZ/Y}$ mice ($n = 4$ to 5 for control diet and $n = 14$ to 16 for HFD). (*G*) Blood glucose concentrations during the GTT and ITT ($n = 8$ to 9 for control diet and $n = 16$ to 18 for HFD). i.p., intraperitoneal. Data are presented as mean ± SEM. $^*P < 0.05$.

(21–23). Secretory vesicles with the coat protein complex II (COPII) mediate transport of newly synthesized proteins from the ER (24–26). *Yipf6* is located on the X chromosome. The protein it encodes colocalizes with the SEC31 homolog A (SEC31A), a COPII coat complex component, so YIPF6 might be involved in trafficking proteins from the ER to the Golgi (20).

We used mice with germline disruption of *Yipf6* (*Klein–Zschocher* [*KLZ*]; $Yipf6^{KLZ/Y}$ mice) by exposure of mice to *N*-ethyl-*N*-nitrosourea (20). In $Yipf6^{KLZ/Y}$ mice, only the *Yipf6* gene is disrupted; when these mice are crossed with transgenic mice that carry a bacterial artificial chromosome that contains the full-length *Yipf6*, the progeny do not have the phenotype of $Yipf6^{KLZ/Y}$ mice (20). We demonstrate that $Yipf6^{KLZ/Y}$ mice are protected from diet-induced obesity, hepatic steatosis, and insulin resistance via increased secretion of FGF21 from hepatocytes. We show that YIPF6 binds to FGF21 in the ER lumen and selectively transfers it into COPII vesicles by interaction with SEC23A. Hepatocyte-specific deletion of *Yipf6* increased the FGF21 level in plasma and reduced diet-induced obesity, hepatic steatosis, and insulin resistance. Moreover, we observed an inverse correlation between the level of YIPF6 in liver and serum levels of FGF21 in overweight patients with NAFLD.

Results

$Yipf6^{KLZ/Y}$ Mice Are Protected from Diet-Induced Obesity and Metabolic Syndrome. $Yipf6^{KLZ/Y}$ mice had lower body weights after 16 wk on the high-fat diet (HFD) compared with mice without disruption of *Yipf6* (wild type [WT]) (Fig. 1 *A*–*C*). Body weights of $Yipf6^{KLZ/Y}$ mice fed the HFD did not differ significantly from those of WT or $Yipf6^{KLZ/Y}$ mice fed a normal chow (control) diet (Fig. 1*A*). $Yipf6^{KLZ/Y}$ mice fed the HFD also had significantly lower weights of subcutaneous (s.c.) white adipose tissue, epididymal white adipose tissue, brown adipose tissue, and liver than WT mice fed the HFD (Fig. 1*D*). There were no differences in food intake or intestinal fat absorption (*SI Appendix*, Fig. S1 *A* and *B*).

Consistent with decreased adiposity, $Yipf6^{KLZ/Y}$ mice on the HFD had better metabolic and endocrine profiles than WT mice on the HFD, based on significantly lower serum levels of total, high-density lipoprotein (HDL), and low-density lipoprotein (LDL) cholesterol (Fig. 1*E*); an increased ratio of high-molecular-weight adiponectin to total adiponectin; and decreased plasma leptin levels (Fig. 1*F*). Adiponectin messenger RNA (mRNA) in white adipose tissue was higher in $Yipf6^{KLZ/Y}$ mice fed the HFD than in WT mice fed the HFD (*SI Appendix*, Fig. S1*C*). Moreover, $Yipf6^{KLZ/Y}$ mice had significantly increased glucose tolerance and insulin sensitivity compared with WT mice fed the HFD, as detected by a glucose tolerance test (GTT) and an insulin tolerance test (ITT) (Fig. 1*G*). $Yipf6^{KLZ/Y}$ and WT mice fed the control diet had comparable glucose tolerance and insulin sensitivity (Fig. 1*G*). These findings indicate that disruption of *Yipf6* protects mice from diet-induced obesity and insulin resistance.

Attenuated Liver Steatosis and Injury in $Yipf6^{KLZ/Y}$ Mice. To assess the role of YIPF6 in steatohepatitis, a more advanced disease than hepatic steatosis (3), mice were additionally fed a high-fat, high-cholesterol diet (HFCD). $Yipf6^{KLZ/Y}$ mice fed the HFCD did not have a significant increase in body weight compared with $Yipf6^{KLZ/Y}$ mice or WT mice fed a control diet (*SI Appendix*, Fig. S1*D*). $Yipf6^{KLZ/Y}$ mice fed the HFCD had lower weights of s.c. white adipose tissue, epididymal white adipose tissue, brown adipose tissue, and liver than WT mice fed the HFCD (*SI Appendix*, Fig. S1*E*). Glucose tolerance was improved in $Yipf6^{KLZ/Y}$ mice fed the HFCD compared with WT mice fed this diet (*SI Appendix*, Fig. S1*F*).

Liver steatosis and steatohepatitis are hepatic manifestations of obesity (3). HFD-induced hepatic steatosis and triglyceride and cholesterol accumulation were reduced in $Yipf6^{KLZ/Y}$ mice (*SI Appendix*, Fig. S2 *A* and *B*). $Yipf6^{KLZ/Y}$ mice also had reduced liver injury after 16 wk on the HFCD, based on their lower plasma level of alanine aminotransferase (*SI Appendix*, Fig. S2*C*). Expression of lipogenesis markers, such as peroxisome proliferator-activated receptor gamma (*Pparg*) and cluster of differentiation 36 (*Cd36*) mRNAs, were decreased in livers of $Yipf6^{KLZ/Y}$ mice compared with livers from WT mice (*SI Appendix*, Fig. S2*D*). Notably, the mRNA expression of peroxisome proliferator-activated receptor alpha (*Ppara*), which can directly regulate FGF21 transcription, was up-regulated by the HFD, whereas no difference was observed between HFD-fed WT and $Yipf6^{KLZ/Y}$ mice (*SI Appendix*, Fig. S2*E*). Functional analyses of liver transcriptomes revealed differences in triglyceride and steroid biosynthesis and PPAR signaling pathways (*SI Appendix*, Fig. S2*F*). Levels of mRNAs, such as fatty acid synthase (*Fasn*), elongation of long chain fatty acids family member 6 (*Elovl6*), lipin1 (*Lpin1*), stearyl CoA desaturase 1 (*Scd1*), stearyl CoA desaturase 2 (*Scd2*), lipoprotein lipase (*Lpl*), and fatty acid binding protein 4 (*Fabp4*), were all lower in $Yipf6^{KLZ/Y}$ mice than WT mice when both strains were fed the HFD (*SI Appendix*, Fig. S2*F*). Disruption of *Yipf6* therefore appears to reduce liver steatosis and injury following the HFD or HFCD.

Increased Lipolysis in White Adipose Tissue of $Yipf6^{KLZ/Y}$ Mice. Adipocytes in $Yipf6^{KLZ/Y}$ mice fed the HFD were smaller than adipocytes in WT mice fed the HFD (Fig. 2*A*). We found no significant differences in mRNA levels of lipogenesis markers, such as *Fasn*, *Pparg*, *Cd36*, or sterol regulatory element-binding protein 1c (*Srebp1c*), in the adipose tissue (*SI Appendix*, Fig. S3*A*). However, mRNA levels of lipolysis markers, including adipose triglyceride lipase (*Atgl*) and hormone sensitive lipase (*Hsl*), were significantly increased in adipose tissue from $Yipf6^{KLZ/Y}$ mice fed the HFD vs. WT mice fed the HFD (Fig. 2*B*). HSL protein was also higher in the white adipose tissue of $Yipf6^{KLZ/Y}$ mice than WT mice fed the HFD (Fig. 2*C*). RALA, which is a Ras family small guanosine triphosphate (GTP)-binding protein, was used as a loading control (27). Consistent with increased lipolysis in $Yipf6^{KLZ/Y}$ mice, HFD-fed $Yipf6^{KLZ/Y}$ mice had higher systemic levels of free fatty acids than HFD-fed WT mice (Fig. 2*D*). These results demonstrate that loss of YIPF6 increases fat lipolysis in white adipose tissue, which might contribute to the reduced body weight and fat mass in $Yipf6^{KLZ/Y}$ mice.

Increased Energy Expenditure and Thermogenesis in Brown Adipose Tissue of $Yipf6^{KLZ/Y}$ Mice. We compared metabolic rates of WT and $Yipf6^{KLZ/Y}$ mice on the HFD. Oxygen consumption and carbon dioxide production rates were significantly higher in $Yipf6^{KLZ/Y}$ mice than WT mice (*SI Appendix*, Fig. S3*B*). There was a lower respiratory exchange ratio in $Yipf6^{KLZ/Y}$ mice, indicating increased use of fat for energy production (*SI Appendix*, Fig. S3*C*). $Yipf6^{KLZ/Y}$ mice were more active than WT mice, as measured by the ambulatory horizontal and vertical counts, potentially contributing to higher energy expenditure by $Yipf6^{KLZ/Y}$ mice (*SI Appendix*, Fig. S3*D*). In line with increased energy expenditure, $Yipf6^{KLZ/Y}$ mice generated more heat, with an ∼0.64 °C higher core body temperature and a higher body temperature after cold exposure (4 °C) (Fig. 2*E* and *SI Appendix*, Fig. S3*E*), indicating augmented adaptive thermogenesis.

Consistent with increased energy expenditure and thermogenesis, lipid accumulation in brown adipose tissue was reduced in HFD-fed and HFCD-fed $Yipf6^{KLZ/Y}$ mice compared with WT mice on the same diet (Fig. 2*F* and *SI Appendix*, Fig. S3*F*). Gene expression analysis showed strong induction of uncoupling protein 1 (*Ucp1*), type 2 deiodinase (*Dio2*), *Hsl*, and *Atgl*, which are involved in thermogenesis and lipolysis, respectively (Fig. 2 *G* and *H*). Expression of the adrenergic receptor, beta 3 (*Adrb3*), a major mediator of adrenergic signaling in adipose tissue, was also consistently increased (Fig. 2*G*). We confirmed increased protein levels of HSL and UCP1 in brown adipose tissue of $Yipf6^{KLZ/Y}$ mice compared with WT mice (Fig. 2*I*). Loss of YIPF6 therefore increases energy expenditure and thermogenesis in brown adipose tissue, which might contribute to the reduced body weight in $Yipf6^{KLZ/Y}$ mice.

Increased Hepatic Secretion of FGF21 Mediates Protective Effects of *Yipf6* Deficiency. $Yipf6^{KLZ/Y}$ mice have a phenotype similar to that of mice expressing an *Fgf21* transgene, characterized by lower

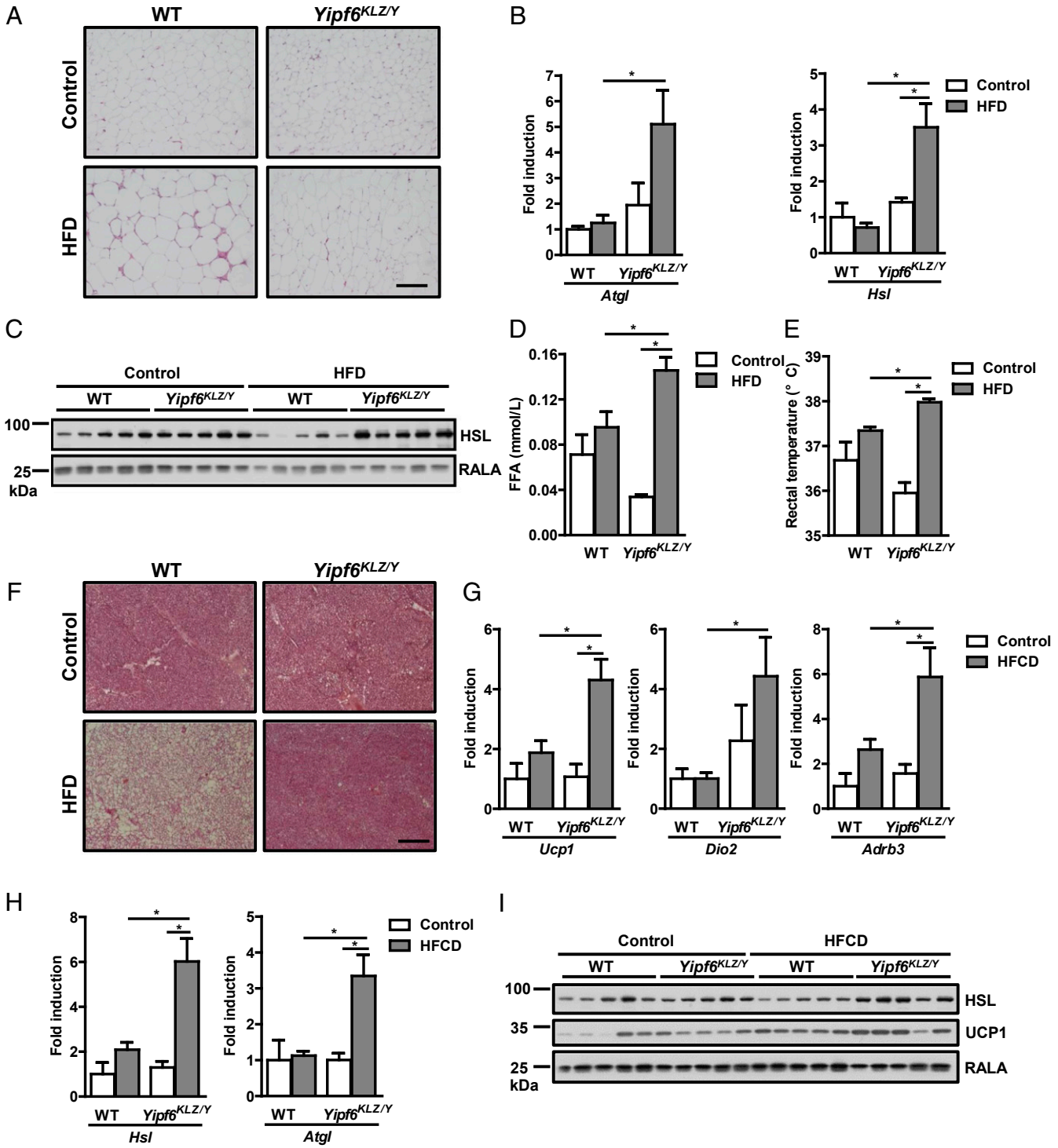

Fig. 2. Disruption of *Yipf6* increases lipolysis in white adipose tissue and thermogenesis in brown adipose tissue. (*A*) Representative images of hematoxylin/eosin (H&E) staining of epididymal fat from HFD-fed WT and *Yipf6*$^{KLZ/Y}$ mice. (*B*) *Atgl* and *Hsl* mRNA levels in white adipose tissue ($n = 3$ to 5 for control diet and $n = 8$ for HFD). (*C*) Immunoblot for HSL and RALA in epididymal fat from WT and *Yipf6*$^{KLZ/Y}$ mice ($n = 5$ per group). (*D*) Plasma free fatty acid (FFA) levels ($n = 4$ to 5 for control diet and $n = 11$ to 13 for HFD). (*E*) Rectal temperatures of 16 wk HFD-fed WT and *Yipf6*$^{KLZ/Y}$ mice at room temperature ($n = 4$ to 5 for control diet and $n = 8$ to 9 for HFD). (*F*) Representative images of H&E-stained brown adipose tissue. Levels of *Ucp1*, *Dio2*, and *Adrb3* mRNAs (*G*) and *Hsl* and *Atgl* mRNAs (*H*) are shown in brown adipose tissue ($n = 4$ to 5 for control diet and $n = 7$ to 10 for HFCD). (*I*) Immunoblot for HSL, UCP1, and RALA in brown adipose tissue from WT and *Yipf6*$^{KLZ/Y}$ mice fed the control diet or HFCD for 16 wk ($n = 5$ per group). Data are presented as mean ± SEM. *$P < 0.05$. (Scale bars, 50 μm.)

body weight gain and increased lipolysis and expression of UCP1, indicating increased thermogenesis and energy expenditure (11, 15, 28). Considering the role of YIPF family members in vesicle trafficking (20, 22, 23), we measured plasma levels of FGF21, which we found to be higher in *Yipf6*$^{KLZ/Y}$ mice compared with WT mice when both were fed the HFD (Fig. 3*A*). Hepatocytes

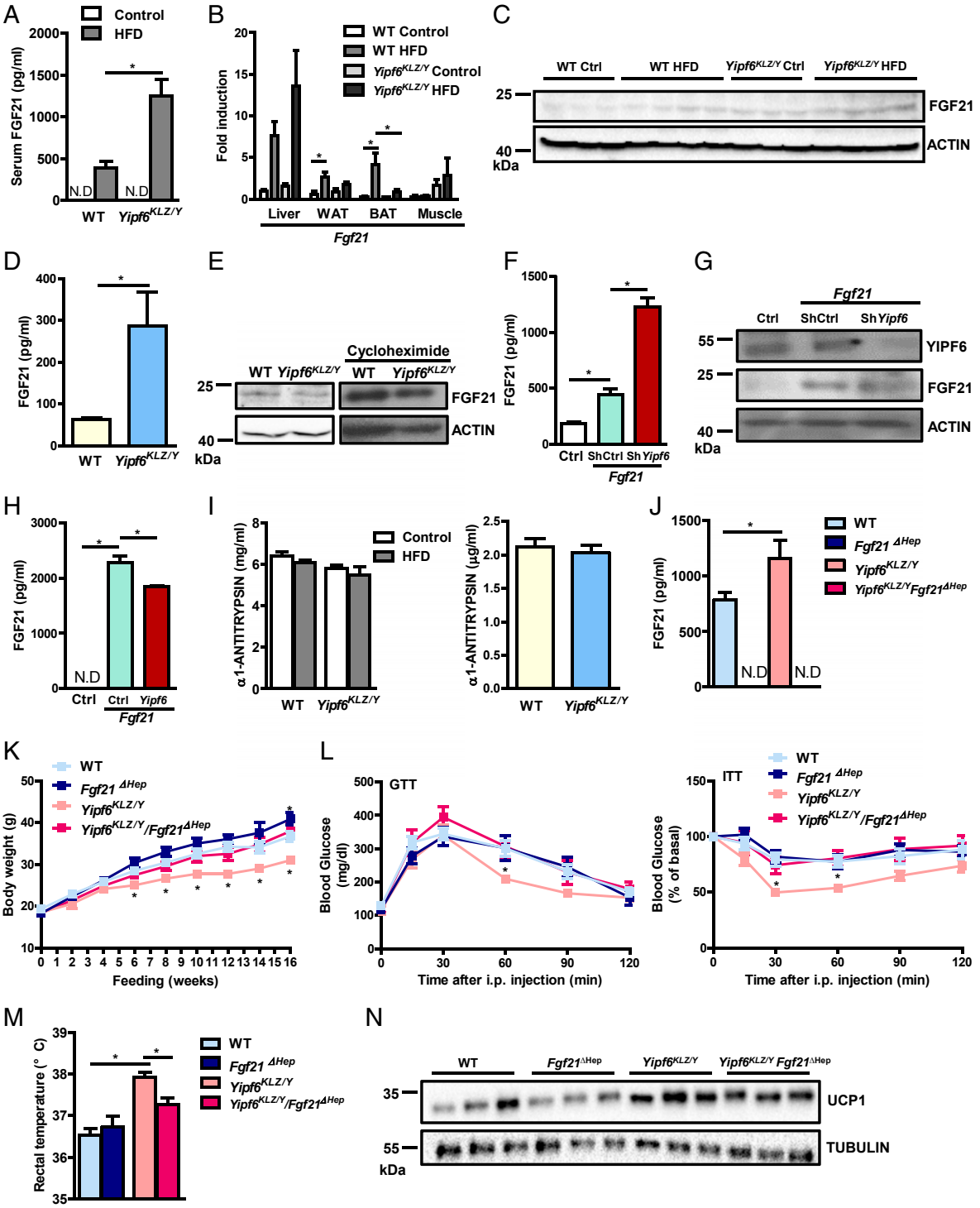

Fig. 3. Disruption of *Yipf6* increases FGF21 secretion by hepatocytes. (*A*–*C*) Mice were fed the HFD for 16 wk. (*A*) Serum level of FGF21 ($n = 5$ per group). N.D., not detected. (*B*) *Fgf21* mRNA in liver, white adipose tissue (WAT), brown adipose tissue (BAT), and muscle ($n = 4$ to 5 for control diet and $n = 8$ to 12 for HFD). (*C*) FGF21 protein in liver extracts ($n = 3$ for control [Ctrl] diet and $n = 4$ for HFD). (*D* and *E*) WT and $Yipf6^{KLZ/Y}$ mice were fed the HFD diet for 16 wk. (*D*) Hepatocytes were isolated, and levels of FGF21 in supernatants were measured ($n = 6$ per group). (*E*) Levels of FGF21 were detected in hepatocytes incubated with or without cycloheximide. (*F* and *G*) AML12 cells were transfected with empty vector (Ctrl) or vectors that expressed FGF21 along with shRNA control (ShCtrl) or shRNA *Yipf6* (Sh*Yipf6*) for 48 h. Levels of FGF21 were measured in cell supernatants (*F*) and in cell extracts (*G*, immunoblot). (*H*) AML12 cells were transfected with empty vector (Ctrl) or vectors that expressed FGF21 or YIPF6 for 24 h, and FGF21 levels were measured in supernatants ($n = 3$). (*I*) Mice were fed the HFD for 16 wk, and levels of A1AT were measured in plasma (*Left*, $n = 5$ per group) and in supernatants of hepatocytes isolated from mice (*Right*, $n = 6$ per group). (*J*–*N*) WT, $Fgf21^{\Delta Hep}$, $Yipf6^{KLZ/Y}$, and $Yipf6^{KLZ/Y}/Fgf21^{\Delta Hep}$ mice were fed the HFD for 16 wk. (*J*) Plasma levels of FGF21 ($n = 6$ for WT and $Fgf21^{\Delta Hep}$ mice, $n = 5$ for $Yipf6^{KLZ/Y}$ and $Yipf6^{KLZ/Y}/Fgf21^{\Delta Hep}$ mice). (*K*) Body weights ($n = 9$ for WT mice, $n = 11$ for $Fgf21^{\Delta Hep}$ mice, $n = 8$ for $Yipf6^{KLZ/Y}$ mice, $n = 9$ for $Yipf6^{KLZ/Y}/Fgf21^{\Delta Hep}$ mice). (*L*) Blood glucose levels in the GTT and ITT ($n = 10$ for WT mice, $n = 10$ to 11 for $Fgf21^{\Delta Hep}$ mice, $n = 5$ to 6 for $Yipf6^{KLZ/Y}$ mice, $n = 6$ to 11 for $Yipf6^{KLZ/Y}/Fgf21^{\Delta Hep}$ mice). i.p., intraperitoneal. (*M*) Rectal temperatures ($n = 7$ for WT mice, $n = 5$ for $Fgf21^{\Delta Hep}$ mice, $n = 10$ for $Yipf6^{KLZ/Y}$ mice, $n = 13$ for $Yipf6^{KLZ/Y}/Fgf21^{\Delta Hep}$ mice). (*N*) Levels of UCP1 protein in brown adipose tissue ($n = 3$ per group). Data are presented as mean ± SEM. $^*P < 0.05$.

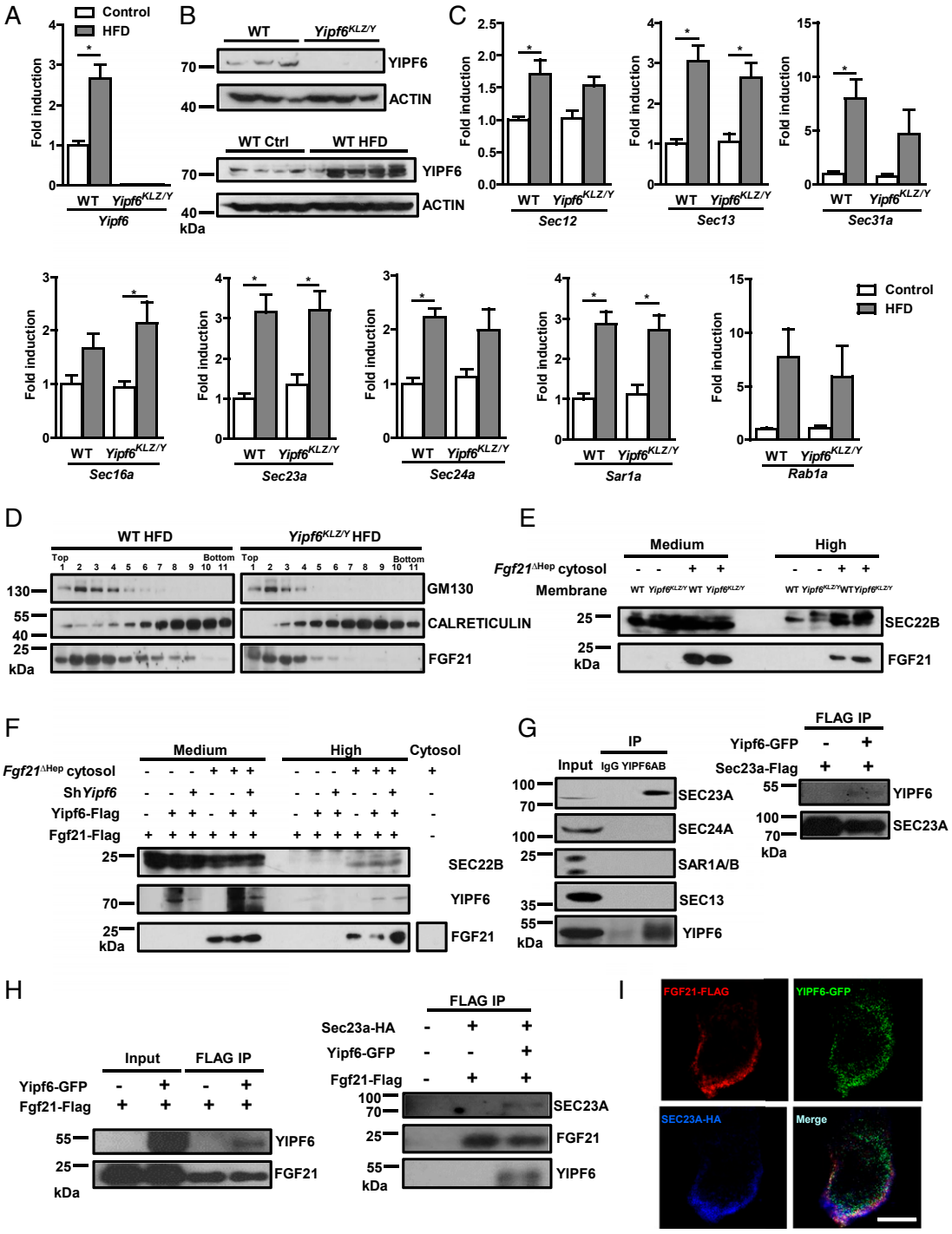

Fig. 4. YIPF6 binds SEC23A and controls packaging of FGF21 into COPII vesicles. (*A–C*) WT and *Yipf6*$^{KLZ/Y}$ mice were fed the control diet or the HFD for 16 wk. (*A*) Levels of *Yipf6* mRNA in liver. (*B*, *Upper*) Hepatocytes were isolated from WT and *Yipf6*$^{KLZ/Y}$ mice fed the control diet, and cellular YIPF6 protein was detected by immunoblot. (*B*, *Lower*) YIPF6 protein in livers of WT mice fed the control (Ctrl) diet and HFD. (*C*) *Sec12*, *Sec13*, *Sec31*a *Sec16a*, *Sec23a*, *Sec24a*, *Sar1a*, and *Rab1a* mRNAs in liver (n = 5 per group). (*D*) WT and *Yipf6*$^{KLZ/Y}$ mice were fed the HFD for 16 wk. Primary hepatocytes were isolated. FGF21 subcellular localization was analyzed in hepatocytes by fractionation of the ER and Golgi. (*E*) In vitro COPII budding assays with primary hepatocytes from WT or *Yipf6*$^{KLZ/Y}$ mice each fed the HFD for 16 wk. (*F*) HEK293T cells overexpressing YIPF6, sh*Yipf6*, or FGF21 for 48 h, providing donor membranes. Liver cytosol from *Fgf21*$^{\Delta Hep}$ mice provided COPII components. The respective medium-speed samples (Medium) and high-speed samples (High, contains COPII vesicles) collected from the budding reaction were resolved on sodium dodecyl sulfate polyacrylamide gel electrophoresis and processed for immunoblotting with SEC22B, FGF21, and YIPF6 antibodies. (*G*, *Left*) Immunoprecipitated (IP) endogenous YIPF6 in AML12 cells and immunoblots for SEC23A, SEC24A, SAR1A/B, SEC13, and YIPF6. (*G*, *Right*) HEK293T cells were transfected with *Yipf6*-GFP and *Sec23a*-Flag constructs for 48 h. Immunoprecipitated SEC23A with Flag beads in HEK293T cells and immunoblots for YIPF6 and SEC23A. (*H*, *Left*) HEK293T cells were transfected with *Yipf6*-GFP and *Fgf21*-Flag constructs for 48 h. FGF21 was immunoprecipitated from HEK293T cells with Flag beads and immunoblot for YIPF6 and FGF21. (*H, Right*) HEK293T cells were transfected with *Yipf6*-GFP, *Fgf21*-Flag, and *Sec23a*-hemagglutinin (HA) for 48 h. FGF21 was immunoprecipitated with Flag beads from HEK293T cells; immunoblot for SEC23A, FGF21, and YIPF6. (*I*) HEK293T cells were transfected with *Fgf21*-Flag, *Yipf6*-GFP, and *Sec23a*-HA for 48 h. Immunofluorescent staining was performed with FGF21 and HA antibodies. Confocal images of FGF21-Flag, YIPF6-GFP, and SEC23A-HA. (Scale bar, 10 μm.) Data are presented as mean ± SEM. *$P < 0.05$.

are the main producers of FGF21 (29). Expression of *Fgf21* mRNA in liver is higher than in adipose tissue (white adipose tissue and brown adipose tissue) and muscle (Fig. 3*B*). However, hepatic levels of *Fgf21* mRNA and FGF21 protein did not differ significantly between WT and *Yipf6*$^{KLZ/Y}$ mice fed the HFD for 16 wk (Fig. 3 *B* and *C*). In addition, primary hepatocytes isolated from WT and *Yipf6*$^{KLZ/Y}$ mice fed the HFD had similar *Fgf21* mRNA levels (*SI Appendix*, Fig. S4*A*); thus, loss of YIPF6 might affect the plasma level of FGF21 after its transcription and translation. Although primary hepatocytes isolated from *Yipf6*$^{KLZ/Y}$ mice fed the control diet secreted less FGF21 than hepatocytes from WT mice fed the control diet (*SI Appendix*, Fig. S4*B*), hepatocytes isolated from HFD-fed *Yipf6*$^{KLZ/Y}$ mice secreted more FGF21 into supernatants than hepatocytes from HFD-fed WT mice (Fig. 3*D*), while cellular levels of FGF21 protein did not differ between WT and *Yipf6*$^{KLZ/Y}$ hepatocytes (Fig. 3 *E*, *Left*). When we used cycloheximide to block protein synthesis, we found that cellular FGF21 protein was similar in hepatocytes isolated from HFD-fed WT and *Yipf6*$^{KLZ/Y}$ mice (Fig. 3 *E*, *Right*). This indicates that YIPF6 does not affect protein degradation or stability.

Knockdown of YIPF6 with small hairpin RNA (shRNA) increased secretion of FGF21 by the mouse hepatocyte cell line AML12 (Fig. 3*F*) but did not affect cellular levels of FGF21 protein (Fig. 3*G*). Furthermore, actinomycin D, which is an inhibitor of transcription and replication (30), was utilized to block *Fgf21* mRNA expression (*SI Appendix*, Fig. S4*C*). Knockdown of YIPF6 increased the secreted FGF21 level in the supernatant compared with controls in the presence of actinomycin D (*SI Appendix*, Fig. S4*D*). Alternatively, overexpression of YIPF6 significantly reduced secretion of FGF21 by these cells (Fig. 3*H*). It is important to note that AML12 cells secrete an endogenous level of FGF21 that is below the limit of detection (or close to the lowest concentration that can be detected), so we had to express FGF21 from a transgene for these experiments (Fig. 3 *F*–*H* and *SI Appendix*, Fig. S4 *C* and *D*) to resemble the increased FGF21 expression during obesity.

FGF21 has an N-terminal signal peptide; we confirmed its transport via COPII vesicles by demonstrating the colocalization of the FGF21 and COPII marker protein SEC31A (19) (*SI Appendix*, Fig. S4*E*). To test whether loss of YIPF6 causes an overall increase in COPII vesicle-mediated transport and secretion, we measured α1-antitrypsin (A1AT or SERPINA1), a protein secreted via the COPII vesicle pathway (31). Levels of A1AT did not differ significantly between plasma from HFD-fed WT vs. *Yipf6*$^{KLZ/Y}$ mice or in supernatants of isolated hepatocytes from HFD-fed WT vs. *Yipf6*$^{KLZ/Y}$ mice (Fig. 3*I*). Loss of YIPF6 promotes secretion specifically of FGF21 from hepatocytes.

To demonstrate that increased FGF21 secretion from hepatocytes protects *Yipf6*$^{KLZ/Y}$ mice from the effects of the HFD, we generated *Yipf6*$^{KLZ/Y}$ mice with hepatocyte-specific disruption of *Fgf21* (*Yipf6*$^{KLZ/Y}$/*Fgf21*$^{\Delta Hep}$). FGF21 was not detectable in plasma from *Yipf6*$^{KLZ/Y}$/*Fgf21*$^{\Delta Hep}$ mice fed the HFD (Fig. 3*J*), demonstrating the disruption of the gene and confirming that hepatocytes are the main source of systemic FGF21. The *Yipf6*$^{KLZ/Y}$/*Fgf21*$^{\Delta Hep}$ mice lost the protection from the effects of the HFD observed in *Yipf6*$^{KLZ/Y}$ mice and became obese, had body weight gain, and developed glucose intolerance and insulin resistance (Fig. 3 *K* and *L* and *SI Appendix*, Fig. S4*F*). *Yipf6*$^{KLZ/Y}$/*Fgf21*$^{\Delta Hep}$ mice had normal body temperatures (Fig. 3*M*) and reduced production of UCP1 protein in brown adipose tissue, compared with *Yipf6*$^{KLZ/Y}$ mice, after 16 wk on the HFD (Fig. 3*N*).

SEC proteins affect selection of proteins for transport via the COPII-mediated secretory pathway from the ER to the Golgi apparatus (25, 32, 33). Mice with a disrupted *Sec24a* gene are not able to secrete proprotein convertase subtilisin/kexin type 9 (PCSK9) (34). PCSK9 is secreted into the plasma by hepatocytes, where it binds to the LDL receptor (LDLR) and promotes its endocytosis and degradation. PCSK9 is therefore a negative regulator of the LDLR (35). Hepatic levels of LDLR are increased in SEC24A-deficient mice, which lowers total plasma cholesterol (34). WT, *Yipf6*$^{KLZ/Y}$, and *Yipf6*$^{KLZ/Y}$/*Fgf21*$^{\Delta Hep}$ mice had comparable plasma levels of PCSK9 following the HFD (*SI Appendix*, Fig. S4*G*). In addition, hepatocytes isolated from HFD-fed WT and *Yipf6*$^{KLZ/Y}$ mice secreted similar amounts of PCSK9 (*SI Appendix*, Fig. S4*H*). So, loss of YIPF6 seems to protect mice from HFD-induced obesity by specifically increasing secretion of FGF21 by hepatocytes.

YIPF6 Limits Sorting of FGF21 into COPII Vesicles. To determine the mechanism by which YIPF6 modulates FGF21 secretion, we measured hepatic gene expression of YIPF1 to YIPF7. Although hepatic expression of most *Yipf* genes, including *Yipf6*, increased in mice on the HFD vs. the control diet (*Yipf2* to *Yipf6*) (Fig. 4 *A* and *B* and *SI Appendix*, Fig. S5*A*), no significant differences in expression of these genes were observed in HFD-fed WT vs. *Yipf6*$^{KLZ/Y}$ mice (Fig. 4*A* and *SI Appendix*, Fig. S5*A*). *Yipf7* was not expressed in liver (36).

FGF21 is secreted via the COPII vesicle pathway, so we investigated hepatic expression of COPII components. Although expression of most proteins involved in the COPII early secretory pathway increased in mice on the HFD compared with the control diet, no significant differences were found between WT and *Yipf6*$^{KLZ/Y}$ mice (Fig. 4*C*). This means that the increase in FGF21 secretion observed in *Yipf6*$^{KLZ/Y}$ mice cannot be attributed to increases in specific COPII components. Confocal imaging showed that YIPF6 localized to the ER and Golgi in mouse hepatocytes, based on colocalization with the ER marker protein calnexin and *cis*-Golgi matrix protein GM130 (*SI Appendix*, Fig. S5*B*), consistent with previous reports (37, 38). We studied ER and Golgi fractions to determine the subcellular distribution of FGF21. A higher amount of FGF21 was present in the ER of hepatocytes isolated from HFD-fed WT mice compared with hepatocytes isolated from HFD-fed *Yipf6*$^{KLZ/Y}$ mice (Fig. 4*D*), although the levels of FGF21 in Golgi fractions were similar. These findings indicate that YIPF6 affects FGF21 secretion at the ER stage.

To explore the role of YIPF6 in secretion of FGF21, we used an in vitro COPII vesicle budding assay. Primary hepatocytes from HFD-induced WT and *Yipf6*$^{KLZ/Y}$ mice, supplied donor membranes, and liver cytosol from *Fgf21*$^{\Delta Hep}$ mice provided the COPII components (34, 36, 39, 40). In the budding assay, we detected more FGF21 in *Yipf6*$^{KLZ/Y}$ membrane-derived COPII vesicles (Fig. 4*E*), which is consistent with the enzyme-linked immunosorbent assay (ELISA) result in Fig. 3*D*. We performed a second COPII vesicle budding assay, in which permeabilized 293T cells expressing YIPF6, sh*Yipf6*, or FGF21 supplied the membrane fraction and liver cytosol from *Fgf21*$^{\Delta Hep}$ mice provided COPII components. In agreement with results from an ELISA (Fig. 3 *F* and *H*), the COPII budding assay demonstrated that overexpression of YIPF6 decreased FGF21 packaging into COPII vesicles, whereas shRNA knockdown of YIPF6 promoted this process (Fig. 4*F*). We also demonstrated that YIPF6 and FGF21 are incorporated into the COPII vesicles and are part of the early secretory pathway (Fig. 4*F*).

We investigated the roles of YIPF6 as a transmembrane protein in the ER (20). To search for YIPF6 interaction partners, YIPF6 was immunoprecipitated from AML12 hepatocytes; the immunoprecipitant was screened with antibodies against COPII coat proteins and RAB1 proteins, which have been reported to mediate COPII vesicle trafficking (41, 42). Although we could not detect an interaction between YIPF6 and SEC24A, SEC13, SAR1A/B, or RAB1A/B (Fig. 4*G* and *SI Appendix*, Fig. S5 *C* and *D*), YIPF6 interacted with SEC23A (Fig. 4*G*). Furthermore, YIPF6 interacted with FGF21 (Fig. 4 *H* and *I*). FGF21 interacted with SEC23A, which required the presence of YIPF6 (Fig. 4 *H*, *Right*). Collectively, these results indicate that YIPF6 selects FGF21 for sorting into COPII vesicles, functioning as a cargo receptor. Through its interaction with SEC23A, YIPF6, together with FGF21, is pulled into budding vesicles. FGF21 sorting and packaging are more efficient in the absence of YIPF6.

Hepatocyte-Specific Deletion of *Yipf6* Increases Systemic FGF21 and Reduces Diet-Induced Obesity and Metabolic Syndrome. To confirm the regulation of FGF21 secretion by YIPF6 in hepatocytes in vivo, we generated a *Yipf6* conditional knockout mouse ($Yipf6^{flox/Y}$). LoxP sites were inserted between exons 1 and 2 and between exons 4 and 5 (*SI Appendix*, Fig. S6 *A* and *B*). To generate a hepatocyte-specific *Yipf6* deletion, AAV8, which has high tropism for hepatocytes, overexpressing Cre recombinase under the hepatocyte-specific albumin promoter was injected into the tail vein of $Yipf6^{flox/Y}$ mice. AAV8-expressing GFP was used as a control vector. AAV8-mediated deletion of *Yipf6* in hepatocytes ($Yipf6^{\Delta Hep}$; Fig. 5*A*) increased plasma levels of FGF21 (Fig. 5*B*), but did not significantly affect *Fgf21* mRNA expression in the liver after 22 wk on the HFD (Fig. 5*C*). $Yipf6^{\Delta Hep}$ mice generated more heat with a higher core body temperature (Fig. 5*D*) and increased UCP1 expression in brown adipose tissue (Fig. 5*E*) compared with $Yipf6^{flox/Y}$ mice injected with AAV8 expressing GFP after 22 wk on HFD. $Yipf6^{\Delta Hep}$ mice showed significantly lower body weight gain (Fig. 5*F*), lower weight of epididymal white adipose tissue (Fig. 5*G*), and attenuated hepatic steatosis (Fig. 5*H*) despite similar food intake (Fig. 5*I*). Moreover, HFD-fed $Yipf6^{\Delta Hep}$ mice had significantly increased glucose tolerance and insulin sensitivity compared with $Yipf6^{flox/Y}$ mice injected with AAV8-expressing GFP, as detected by the GTT and ITT (Fig. 5*J*). These findings indicate that deletion of *Yipf6* specifically in hepatocytes protects mice from diet-induced obesity and features of the metabolic syndrome by increasing FGF21 secretion.

Inverse Correlation between Level of YIPF6 in Liver and Serum Level of FGF21 in Patients with NAFLD. We examined the association between hepatic levels of YIPF6 and serum levels of FGF21 in patients with NAFLD. We obtained liver tissues from 16 patients with biopsy-proven NAFLD (liver biopsies are not available from patients without liver disease) (*SI Appendix*, Tables S1 and S2). Levels of YIPF6 in liver tissues correlated inversely with patients' serum level of FGF21 (Fig. 6 *A* and *B*). Furthermore, hepatic levels of YIPF6 correlated with the extent of liver steatosis (Fig. 6 *A* and *C*).

Discussion

We found $Yipf6^{KLZ/Y}$ mice to have increased lipolysis, thermogenesis, and energy expenditure and to be protected from diet-induced features of the metabolic syndrome, including obesity and hepatic steatosis. We investigated the role of YIPF family members in vesicle transport between the ER and Golgi apparatus (20, 22, 23) and found that increased hepatocyte secretion of FGF21 mediates the protection of $Yipf6^{KLZ/Y}$ mice from the effects of the HFD. Hepatocyte-specific deletion of *Yipf6* confirmed our findings.

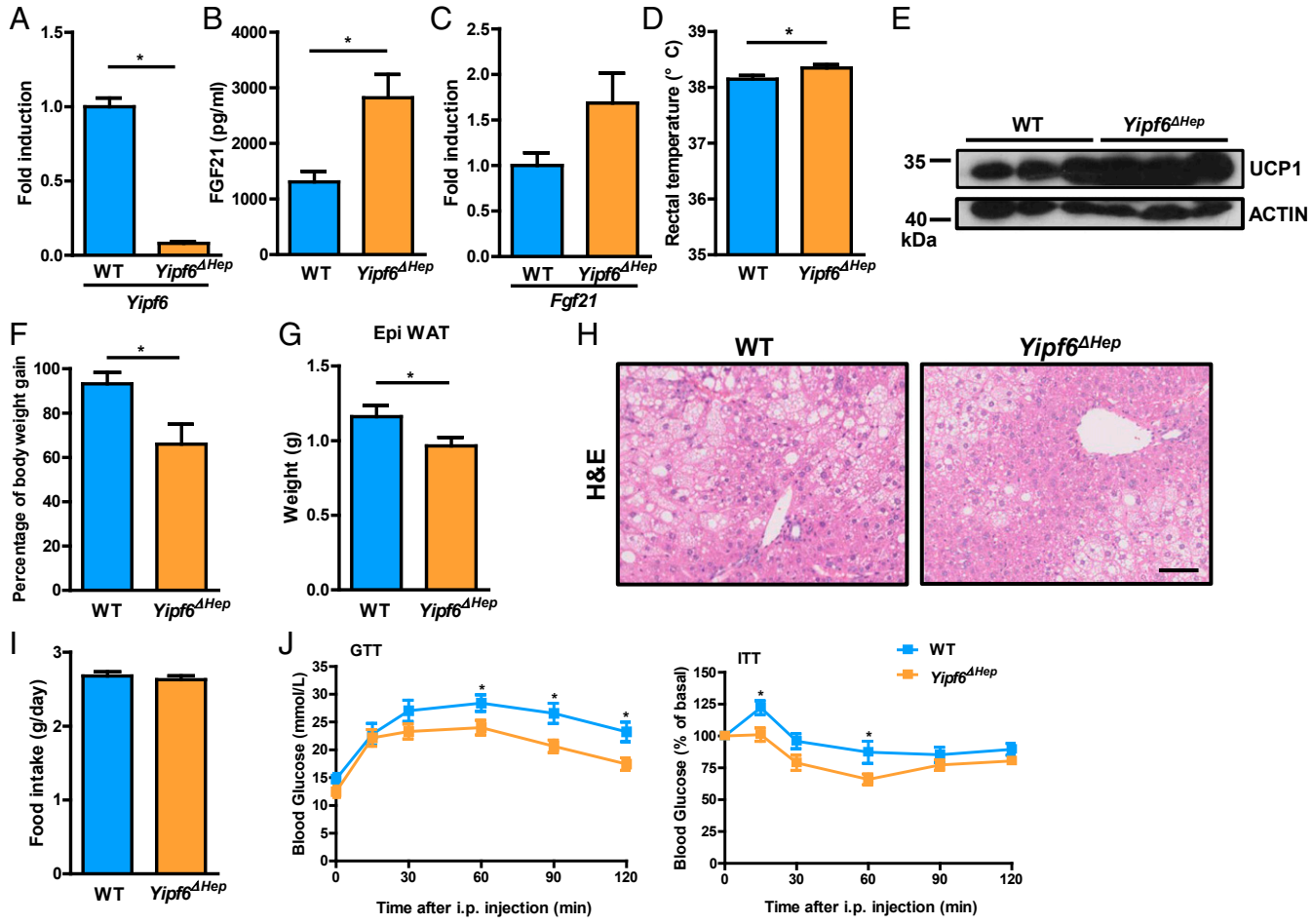

Fig. 5. Hepatocyte-specific deletion of *Yipf6* protects mice from diet-induced obesity and features of the metabolic syndrome. $Yipf6^{flox/Y}$ mice were fed the HFD for 5 wk, injected with AAV8 encoding GFP (WT; $n = 9$ to 16) or Cre recombinase ($Yipf6^{\Delta Hep}$; $n = 15$ to 20) under the hepatocyte-specific albumin promoter through the tail vein. After injection, mice were fed the HFD for an additional 22 wk. (*A*) *Yipf6* mRNA in liver. (*B*) Plasma level of FGF21. (*C*) *Fgf21* mRNA in liver. (*D*) Rectal temperature. (*E*) UCP1 protein expression in brown adipose tissue ($n = 3$ for WT mice, $n = 3$ for $Yipf6^{\Delta Hep}$ mice). (*F*) Percentage of body weight gain. (*G*) Weight of epididymal white adipose tissue (Epi WAT). (*H*) Representative hematoxylin/eosin (H&E)-stained liver sections. (Scale bar, 50 μm.) (*I*) Food intake. (*J*) Blood glucose concentrations during the GTT and ITT ($n = 7$ to 8 for WT mice, $n = 8$ for $Yipf6^{\Delta Hep}$ mice). i.p., intraperitoneal. Data are presented as mean ± SEM. $^*P < 0.05$.

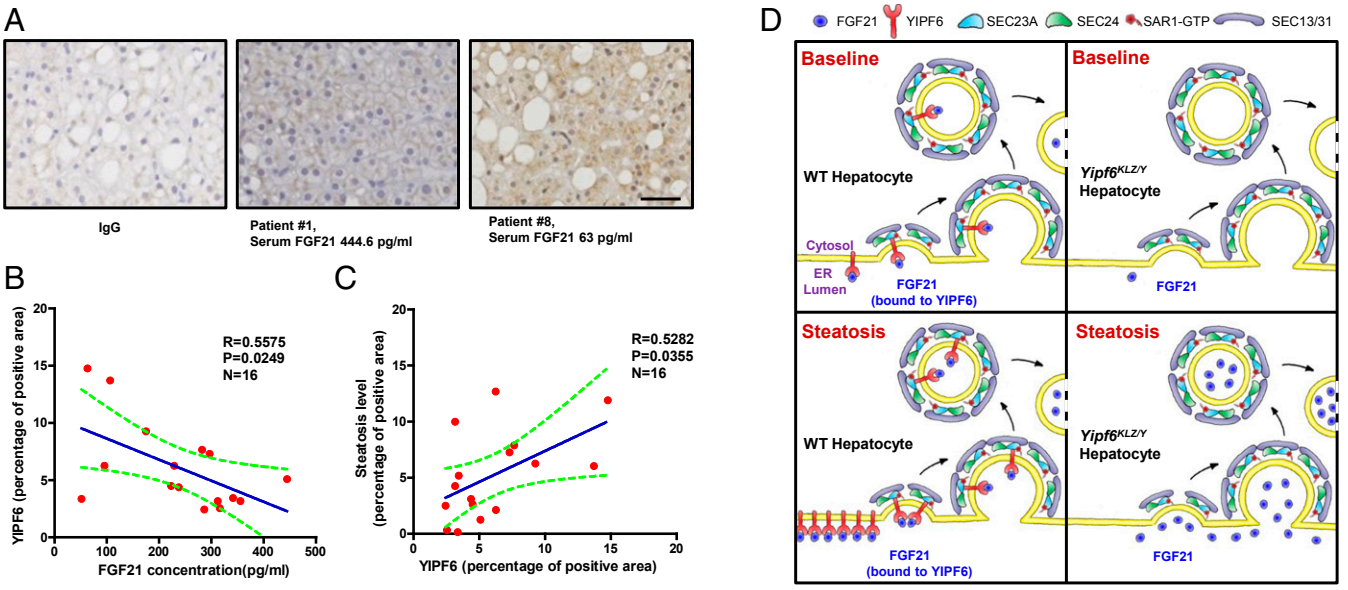

Fig. 6. Relationships among hepatic YIPF6, serum FGF21, and steatosis in patients with NAFLD. (*A*) Representative images of hepatic tissues from patients with NAFLD, with immunohistochemistry for immunoglobulin G (IgG; control) or YIPF6. (Scale bar, 50 μm.) (*B*) Inverse correlation between hepatic level of YIPF6 and serum level of FGF21 in patients with NAFLD. (*C*) Correlation of hepatic YIPF6 with steatosis in patients with NAFLD. (*D*) Model for YIPF6 as a cargo receptor for FGF21 budding. (*Left Upper*) Under baseline conditions with low FGF21 (blue circle) and YIPF6 protein (red) in the ER of WT hepatocytes, the small amount of FGF21 is bound to YIPF6 in the ER lumen and is secreted via COPII vesicles. YIPF6 is using SEC23A (light blue) as a guide into budding vesicles. (*Right Upper*) In the absence of YIPF6, the small amount of FGF21 cannot easily enter the budding vesicle without the selection and sorting of YIPF6. In both situations, secreted FGF21 levels are low in the systemic circulation under healthy conditions. (*Left Lower*) During steatosis and obesity, YIPF6 and FGF21 increase in the ER of WT hepatocytes. YIPF6 binds FGF21 in the ER lumen and interacts with SEC23A, keeping FGF21 from an unrestricted flow into COPII vesicles. The selection of FGF21 by YIPF6 and packaging of FGF21 into COPII vesicles determine the amount of secreted FGF21. (*Right Lower*) In *Yipf6*$^{KLZ/Y}$ hepatocytes, the absence of YIPF6 allows FGF21 to escape retention by YIPF6 and facilitates FGF21 entering into COPII vesicles at prevailing luminal ER concentrations, leading to increased secretion of FGF21.

Using ER-Golgi fractionation and COPII budding assays, we demonstrated that FGF21 is secreted via COPII vesicles and that YIPF6 is also present in COPII vesicles. YIPF6 is a transmembrane-spanning protein that contains a C-terminal domain with 5 transmembrane domains and a soluble, cytoplasmic N-terminal domain (20). We provided evidence for the interaction between YIPF6 and FGF21. Our findings indicate that the ER transmembrane protein YIPF6 might function as a trafficking receptor for FGF21 because it selects FGF21 for packaging into COPII vesicles in the ER.

By screening proteins involved in the early secretory COPII pathway, we found YIPF6 to interact with SEC23A, but not with other proteins in this pathway. SEC23A is the GTPase-activating protein (GAP) for SAR1, which is a small GTPase that initiates COPII coat assembly (25). SEC23A regulates coat assembly and vesicle trafficking by interacting with a variety of proteins (43, 44). The interaction between YIPF6 and SEC23A provides a physical connection between YIPF6 and COPII vesicles. Immunofluorescence analyses confirmed the colocalization of FGF21, YIPF6, and SEC23A. The interaction between FGF21 and SEC23A could not be detected in the absence of YIPF6, indicating that YIPF6 functions as a transmembrane bridge between the cytosol and the ER lumen. Interestingly, YIPF5, another member of mammalian YIPFs, also interacts with SEC23 (36), indicating the possible overlap in functions of YIPF family members.

Our results indicate that under baseline, nonobese conditions, with low levels of FGF21 and YIPF6 protein in the ER of hepatocytes, the small amount of FGF21 is bound to YIPF6 in the ER lumen and secreted via COPII vesicles. YIPF6 uses SEC23A as a guide into budding vesicles. Secreted levels of FGF21 are low in the systemic circulation of healthy individuals (45). During obesity, when YIPF6 and FGF21 increase in the ER, FGF21 bound to YIPF6 is secreted into COPII vesicles under the guidance of SEC23A, which is also increased in obesity. Therefore, the rate-limiting step for FGF21 secretion is the selection of FGF21 by YIPF6 and packaging of FGF21 into budding vesicles with the guidance of SEC23A. In the absence of YIPF6, FGF21 packaging into COPII transport vesicles is increased during obesity, as we have shown using the COPII budding assay. Because of the higher lumen concentration of unbound FGF21 in the ER, the gradient from the ER to budding vesicles increases, resulting in a flow from the ER lumen into the vesicles; this likely allows for increased secretion of FGF21 (Fig. 6*D*). Alternatively, other adaptor proteins might be more efficient to transport FGF21 into budding vesicles in the absence of YIPF6. Additional studies are needed to further evaluate this possibility.

We confirmed that YIPF6 is not required for general COPII vesicle formation, because secretion of other proteins via the early COPII pathway (A1AT and PCSK9) does not increase in the absence of YIPF6. It will also be important to determine the fate of YIPF6 in COPII vesicles, how YIPF6 releases FGF21 into the Golgi, and how it eventually returns to the ER via the COPI pathway (46). Importantly, this regulatory mechanism seems to be conserved in humans, because we found an inverse correlation between levels of YIPF6 on liver biopsies and FGF21 in serum from patients with NAFLD.

FGF21 has attracted much attention in the field of obesity research, and lately in NAFLD research, and it might be developed as a treatment for these diseases (10, 47, 48). LY2405319, an engineered variant of FGF21, reduced features of obesity and related metabolic syndrome in patients with type 2 diabetes (16, 49). Furthermore, a long-acting FGF21 analog, PF-05231023, reduced body weight and improved dyslipidemia in obese patients with type 2 diabetes (50).

However, the potential side effects of FGF21 therapy, such as bone loss, are a concern (50). A phase 2 clinical trial found that treatment with pegylated FGF21 (BMS-986036) decreased the hepatic fat fraction, improved biomarkers of fibrosis, and reduced liver injury in patients with progressive nonalcoholic steatohepatitis (51). No treatment-related side effects were reported. This is consistent with our observed correlation between hepatic YIPF6 and

steatosis in human liver, although we could not find a correlation between hepatic YIPF6 and body mass index (*SI Appendix*, Fig. S7*A*). One reason for this could be that our study required liver tissue to measure YIPF6 expression. Therefore, our study enrolled patients with liver disease, who had a medical indication to undergo liver biopsy. Although most of the included patients met the criteria for being overweight, only 3 patients were obese and 2 patients were diagnosed with lean NAFLD.

We demonstrate that mice with disruption of *Yipf6* are resistant to diet-induced features of the metabolic syndrome, including obesity and hepatic steatosis, through increased secretion of FGF21 by hepatocytes. We report that YIPF6 is a cargo receptor that becomes a rate-limiting molecule in the FGF21 secretory pathway during development of obesity. Considering the ability of FGF21 analogs to reduce features of obesity in humans, strategies to reduce or disrupt the activity of YIPF6 might be developed for treatment of obesity and NAFLD. Agents that block YIPF6 could promote release of endogenous FGF21 from hepatocytes to reduce the metabolic effects of obesity.

Materials and Methods

All animal studies were reviewed and approved by the Institutional Animal Care and Use Committee of the University of California, San Diego and the Institutional Animal Care and Use Committee of China Pharmaceutical University, Nanjing, China. The human study protocol was approved by the Ethics Committee of the Beijing Ditan Hospital, Capital Medical University, China, and a written informed consent was signed by each participant after the nature and possible consequences of the studies were explained. All of the methods, including those involving mice, human samples, cell lines and primary hepatocytes, triglycerides and cholesterol measurement in liver and feces, plasma assays, GTT and ITT, indirect calorimetry, histology, immunohistochemistry, immunofluorescence analysis, immunoprecipitation assay, coimmunoprecipitation assay, immunoblotting, protein stability experiments, actinomycin D treatment, subcellular fractionation, COPII budding assay, real-time PCR, RNA sequencing, quantification, and statistical analysis, are described in *SI Appendix*, *Supplementary Methods*.

ACKNOWLEDGMENTS. We thank Drs. Randy Schekman (University of California, Berkeley), Peter Novick (University of California San Diego), and Liang Ge (Tsinghua University, China) for helpful discussions, and Drs. Peng Wang and Lei Sun (Beijing Ditan Hospital of Capital Medical University) for help in preparing the human liver tissues. This study was supported, in part, by the National Natural Science Foundation of China (Grant 81700748), "Double First-Class" University Project (Grants CPU2018GF10 and CPU2018GY31), and National Key R&D Program of China (Grant 2018YFC1704905 to L.W.). This study was also supported by NIH Grant R01 AA020703 (to B.S.).

1. WHO, *Obesity and Overweight* (World Health Organization, 2017).
2. A. Afshin *et al*.; GBD 2015 Obesity Collaborators, Health effects of overweight and obesity in 195 countries over 25 years. *N. Engl. J. Med.* **377**, 13–27 (2017).
3. Z. Younossi *et al*., Global burden of NAFLD and NASH: Trends, predictions, risk factors and prevention. *Nat. Rev. Gastroenterol. Hepatol.* **15**, 11–20 (2018).
4. R. C. Meex *et al*., Fetuin B is a secreted hepatocyte factor linking steatosis to impaired glucose metabolism. *Cell Metab.* **22**, 1078–1089 (2015).
5. A. Kharitonenkov *et al*., FGF-21/FGF-21 receptor interaction and activation is determined by betaKlotho. *J. Cell. Physiol.* **215**, 1–7 (2008).
6. Y. Ogawa *et al*., BetaKlotho is required for metabolic activity of fibroblast growth factor 21. *Proc. Natl. Acad. Sci. U.S.A.* **104**, 7432–7437 (2007).
7. M. Suzuki *et al*., betaKlotho is required for fibroblast growth factor (FGF) 21 signaling through FGF receptor (FGFR) 1c and FGFR3c. *Mol. Endocrinol.* **22**, 1006–1014 (2008).
8. K. Fon Tacer *et al*., Research resource: Comprehensive expression atlas of the fibroblast growth factor system in adult mouse. *Mol. Endocrinol.* **24**, 2050–2064 (2010).
9. Q. Gong *et al*., Fibroblast growth factor 21 improves hepatic insulin sensitivity by inhibiting mammalian target of rapamycin complex 1 in mice. *Hepatology* **64**, 425–438 (2016).
10. J. Zhang, Y. Li, Fibroblast growth factor 21, the endocrine FGF pathway and novel treatments for metabolic syndrome. *Drug Discov. Today* **19**, 579–589 (2014).
11. A. Kharitonenkov *et al*., FGF-21 as a novel metabolic regulator. *J. Clin. Invest.* **115**, 1627–1635 (2005).
12. E. D. Berglund *et al*., Fibroblast growth factor 21 controls glycemia via regulation of hepatic glucose flux and insulin sensitivity. *Endocrinology* **150**, 4084–4093 (2009).
13. J. Xu *et al*., Fibroblast growth factor 21 reverses hepatic steatosis, increases energy expenditure, and improves insulin sensitivity in diet-induced obese mice. *Diabetes* **58**, 250–259 (2009).
14. T. Coskun *et al*., Fibroblast growth factor 21 corrects obesity in mice. *Endocrinology* **149**, 6018–6027 (2008).
15. B. M. Owen *et al*., FGF21 acts centrally to induce sympathetic nerve activity, energy expenditure, and weight loss. *Cell Metab.* **20**, 670–677 (2014).
16. G. Gaich *et al*., The effects of LY2405319, an FGF21 analog, in obese human subjects with type 2 diabetes. *Cell Metab.* **18**, 333–340 (2013).
17. M. A. Sánchez-Garrido *et al*., Fibroblast activation protein (FAP) as a novel metabolic target. *Mol. Metab.* **5**, 1015–1024 (2016).
18. V. Jimenez *et al*., FGF21 gene therapy as treatment for obesity and insulin resistance. *EMBO Mol. Med.* **10**, e8791 (2018).
19. M. Zhang, R. Schekman, Cell biology. Unconventional secretion, unconventional solutions. *Science* **340**, 559–561 (2013).
20. K. Brandl *et al*., Yip1 domain family, member 6 (Yipf6) mutation induces spontaneous intestinal inflammation in mice. *Proc. Natl. Acad. Sci. U.S.A.* **109**, 12650–12655 (2012).
21. M. Calero, N. J. Winand, R. N. Collins, Identification of the novel proteins Yip4p and Yip5p as Rab GTPase interacting factors. *FEBS Lett.* **515**, 89–98 (2002).
22. N. Segev, J. Mulholland, D. Botstein, The yeast GTP-binding YPT1 protein and a mammalian counterpart are associated with the secretion machinery. *Cell* **52**, 915–924 (1988).
23. X. Yang, H. T. Matern, D. Gallwitz, Specific binding to a novel and essential Golgi membrane protein (Yip1p) functionally links the transport GTPases Ypt1p and Ypt31p. *EMBO J.* **17**, 4954–4963 (1998).
24. M. J. Kuehn, J. M. Herrmann, R. Schekman, COPII-cargo interactions direct protein sorting into ER-derived transport vesicles. *Nature* **391**, 187–190 (1998).
25. E. A. Miller, R. Schekman, COPII–A flexible vesicle formation system. *Curr. Opin. Cell Biol.* **25**, 420–427 (2013).
26. R. Schekman, L. Orci, Coat proteins and vesicle budding. *Science* **271**, 1526–1533 (1996).
27. S. M. Reilly *et al*., A subcutaneous adipose tissue-liver signalling axis controls hepatic gluconeogenesis. *Nat. Commun.* **6**, 6047 (2015).
28. X. Ding *et al*., βKlotho is required for fibroblast growth factor 21 effects on growth and metabolism. *Cell Metab.* **16**, 387–393 (2012).
29. F. G. Schaap, A. E. Kremer, W. H. Lamers, P. L. Jansen, I. C. Gaemers, Fibroblast growth factor 21 is induced by endoplasmic reticulum stress. *Biochimie* **95**, 692–699 (2013).
30. Y. Zhao *et al*., The lncRNA MACC1-AS1 promotes gastric cancer cell metabolic plasticity via AMPK/Lin28 mediated mRNA stability of MACC1. *Mol. Cancer* **17**, 69 (2018).
31. B. Nyfeler *et al*., Identification of ERGIC-53 as an intracellular transport receptor of alpha1-antitrypsin. *J. Cell Biol.* **180**, 705–712 (2008).
32. J. Dancourt, C. Barlowe, Protein sorting receptors in the early secretory pathway. *Annu. Rev. Biochem.* **79**, 777–802 (2010).
33. J. G. D'Arcangelo, K. R. Stahmer, E. A. Miller, Vesicle-mediated export from the ER: COPII coat function and regulation. *Biochim. Biophys. Acta* **1833**, 2464–2472 (2013).
34. X. W. Chen *et al*., SEC24A deficiency lowers plasma cholesterol through reduced PCSK9 secretion. *eLife* **2**, e00444 (2013).
35. K. N. Maxwell, E. A. Fisher, J. L. Breslow, Overexpression of PCSK9 accelerates the degradation of the LDLR in a post-endoplasmic reticulum compartment. *Proc. Natl. Acad. Sci. U.S.A.* **102**, 2069–2074 (2005).
36. B. L. Tang *et al*., A membrane protein enriched in endoplasmic reticulum exit sites interacts with COPII. *J. Biol. Chem.* **276**, 40008–40017 (2001).
37. T. Kranjc *et al*., Functional characterisation of the YIPF protein family in mammalian cells. *Histochem. Cell Biol.* **147**, 439–451 (2017).
38. A. Shakoori *et al*., Identification of a five-pass transmembrane protein family localizing in the Golgi apparatus and the ER. *Biochem. Biophys. Res. Commun.* **312**, 850–857 (2003).
39. J. Kim *et al*., Biogenesis of gamma-secretase early in the secretory pathway. *J. Cell Biol.* **179**, 951–963 (2007).
40. L. Yuan, S. Baba, K. Bajaj, R. Schekman, Cell-free generation of COPII-coated procollagen I carriers. *Bio Protoc.* **7**, e2450 (2017).
41. B. B. Allan, B. D. Moyer, W. E. Balch, Rab1 recruitment of p115 into a cis-SNARE complex: Programming budding COPII vesicles for fusion. *Science* **289**, 444–448 (2000).
42. S. L. Schwartz, C. Cao, O. Pylypenko, A. Rak, A. Wandinger-Ness, Rab GTPases at a glance. *J. Cell Sci.* **120**, 3905–3910 (2007).
43. J. C. Fromme, L. Orci, R. Schekman, Coordination of COPII vesicle trafficking by Sec23. *Trends Cell Biol.* **18**, 330–336 (2008).
44. C. Lord *et al*., Sequential interactions with Sec23 control the direction of vesicle traffic. *Nature* **473**, 181–186 (2011).
45. A. Mutanen *et al*., Serum FGF21 increases with hepatic fat accumulation in pediatric onset intestinal failure. *J. Hepatol.* **60**, 183–190 (2014).
46. M. C. Lee, E. A. Miller, J. Goldberg, L. Orci, R. Schekman, Bi-directional protein transport between the ER and Golgi. *Annu. Rev. Cell Dev. Biol.* **20**, 87–123 (2004).
47. A. M. Diehl, C. Day, Cause, pathogenesis, and treatment of nonalcoholic steatohepatitis. *N. Engl. J. Med.* **377**, 2063–2072 (2017).
48. A. Kharitonenkov, A. C. Adams, Inventing new medicines: The FGF21 story. *Mol. Metab.* **3**, 221–229 (2013).
49. A. Kharitonenkov *et al*., Rational design of a fibroblast growth factor 21-based clinical candidate, LY2405319. *PLoS One* **8**, e58575 (2013).
50. S. Talukdar *et al*., A long-acting FGF21 molecule, PF-05231023, decreases body weight and improves lipid profile in non-human primates and type 2 diabetic subjects. *Cell Metab.* **23**, 427–440 (2016).
51. A. Sanyal *et al*., BMS-986036 (pegylated FGF21) in patients with non-alcoholic steatohepatitis: A phase 2 study. *J. Hepatol.* **66** (suppl), S89–S90 (2017).